17th World Conference on Earthquake Engineering, 17WCEE
Sendai, Japan - September 13th to 18th 2020

Behavior of BFRP Tendon Systems Under Cyclic Loading and Its Influence on the Dual-Tube SC-BRB Hysteretic Performance

Q. Xie[1], Z. Zhou[2]

[1] *Lecturer, Guizhou Institute of Technology, School of Civil Engineering, xieqinqqq@sina.com*
[2] *Professor, Southeast University, Key Laboratory of Concrete and Prestressed Concrete Structures of the Ministry of Education, seuhj@163.com*

Abstract

Basalt fiber-reinforced polymer (BFRP) is an ideal pretensioned tendon material due to its corrosion resistance, light weight and high elongation. BFRP has been applied to the self-centering buckling-restrained brace (SC-BRB). The performance of the pretensioned tendons is critical to the control of the residual deformation of the SC-BRB. However, the current research on the performance of BFRP tendon systems mainly focuses on the long-term dead load; few studies have been conducted on the large strain cycle loading of the pretensioned tendon in the self-centering brace under earthquake action. In addition, during a previous SC-BRB experiment, although the BFRP tendon did not cause anchorage slippage, pretension loss occurred, and the cause was not determined. Considering the above problems, in this paper, cyclic tensile tests were conducted on multiple sets of BFRP tendon systems. The ultimate elongation rate was exceeded 2.5%, and the elastic modulus changed little during the loading process. Based on the experimental results, the pretension loss of SC-BRB was due to the colloid in the anchor being deformed under cyclic loading, and the regression formula of the colloidal deformation of the anchor is established. According to the results of a quasi-static experiment on SC-BRB, the BFRP tendon can provide a reliable self-centering restoring force for the brace. When loaded into the axial deformation at 2.5% displacement angle, the residual deformation of the brace remains effectively controlled, and the accuracy of estimating the pretension loss based on the regression formula of the anchor colloidal deformation is demonstrated. Finally, a rheological model that can accurately describe the hysteresis performance of SC-BRB and consider the pretension loss is established. The hysteretic behavior analysis of SC-BRB that is based on rheological model demonstrates that the anchor colloidal deformation will lead to a decrease in the brace bearing capacity and an increase in the residual deformation and that the effect will strengthen with the increase in the displacement amplitude.

Keywords: Self-centering ; Pretensioned tendon ; Cyclic loading ; Pretension loss; Hysteretic performance

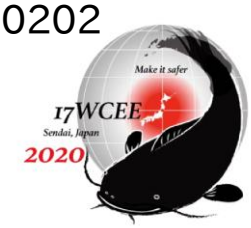

1. Introduction

A resilient structure is a structure that can be quickly restored after an earthquake without repair or with only minor repair[1]. At the NEES/E-Defense Earthquake Engineering Conference in 2009, "Resilient City" was proposed as the future direction of cooperation in the field of seismic engineering[2]. Studies have demonstrated that the structural residual deformation that is caused by the plastic energy consumption of the components will increase the difficulty and time of structural repair and will affect production and life after the earthquake[3]. A self-centering structural system can eliminate the residual deformation of the structure, and is an effective technical means for improving the reparability of the structure. At present, many self-centering structural systems and members have been proposed. Among them, the self-centering brace has better development prospects because its installation is similar to that of conventional braces, which reduces the difficulty of structural design and construction. There are many approaches for realizing self-centering mechanisms for a brace (e.g., a shape memory alloy (SMA)[4] or a disc spring[5]) and tube-pretensioned rod (TPR) self-centering systems[6] that are based on posttensioned prestress technology have been widely studied due to their simple structure and stable performance. Miller et al.[7] combined the TPR system with buckling-restrained brace (BRB), adopted SMA bars as the pretensioned tendons and proposed the structure of a self-centering BRB (SC-BRB). Basalt fiber-reinforced polymer (BFRP) has the characteristics of light weight, corrosion resistance, high strength and high elongation[8] and its cost is much lower than that of SMA. Therefore, Zhou et al.[9] used it as a pretensioned tendon and proposed a dual-tube SC-BRB. However, during quasi-static tests of the brace specimens, although the BFRP tendons did not cause anchorage slippage, the pretension loss occurred during the cyclic loading process and the cause of the loss was not clear[10].

The pretensioned tendon is a key component that provides resilience to the self-centering structure and its performance can affect the reparability of the structure. Therefore, many scholars have studied its performance. Christopoulos et al.[6] performed a cyclic tensile test on an aramid tendon and found that the cyclic modulus of the aramid tendon was approximately 1.4 times that of the monotonic modulus. Chou and Chung[11] uses high-strength steel tendons as the tensioning elements. The cyclic tensile test shows that these steel tendons exhibit a linear elastic material property when the strain is less than 1%. When the tensile force exceeds the maximum load in the previous period, the anchor and the steel tendon will produce relative slip. Bruce and Eatherton[12] conducted a performance study on the posttensioning strand and determined the regression equation of the nonlinear performance and anchor slip of the specimen during cyclic loading. Various types of anchors have been developed for BFRP tendons[13, 14]. Since the compression stress causes the ultimate strength of the BFRP tendons to decrease, the bonding anchor can increase the ultimate strength of the BFRP tendons by 5% to 15%[15] compared to the friction anchor and the wedge anchor. Shi et al.[16] demonstrates that the BFRP tendons with bonding anchors will cause pretension loss due to the creep of the fiber and the deformation of the epoxy resin in the anchorage under a long-term constant load. The above research on the performance of the BFRP tendons mainly considers the case of a constant load; few studies have been conducted on the cyclic tension of the pretensioned tendons in the self-centering structure.

The objective of this investigation is to understand the cyclic behavior of BFRP tendon systems with bonding anchors. This paper examines the following three aspects: (1) the properties of the tendons and anchors of BFRP tendon systems under cyclic loading and the causes of the loss of pretension, (2) the hysteresis behavior of SC-BRB with BFRP tendons and the performance of tendon systems during brace deformation, and (3) the establishment of a rheological model that can describe the hysteresis performance of SC-BRB and consider the pretension loss.

2. Concept of the Dual-Tube SC-BRB

The configuration of the dual-tube SC-BRB[10] is illustrated in Fig. 1(a) and consists of two main parts: the energy dissipation system BRB and the self-centering system (SC). The energy dissipation system consists of two core plates, which consume energy via yield deformation; filled plates; and an inner tube and an outer tube, which prevent the core plate from buckling. The self-centering system consists of an inner tube, an outer tube, end plates, and BFRP tendons. The left end of the inner tube is welded to the left ends of the

© The 17th World Conference on Earthquake Engineering

core plates and the right end of the outer tube is welded to the right ends of the core plates. The BFRP tendons are arranged in the inner tube and the two ends are anchored onto the two end plates. Regardless of whether the brace is tensioned or compressed, the end plates on both sides always drive the extension of BFRP tendons to provide the restoring force for self-centering (Fig. 1(b) and Fig.1(c)).

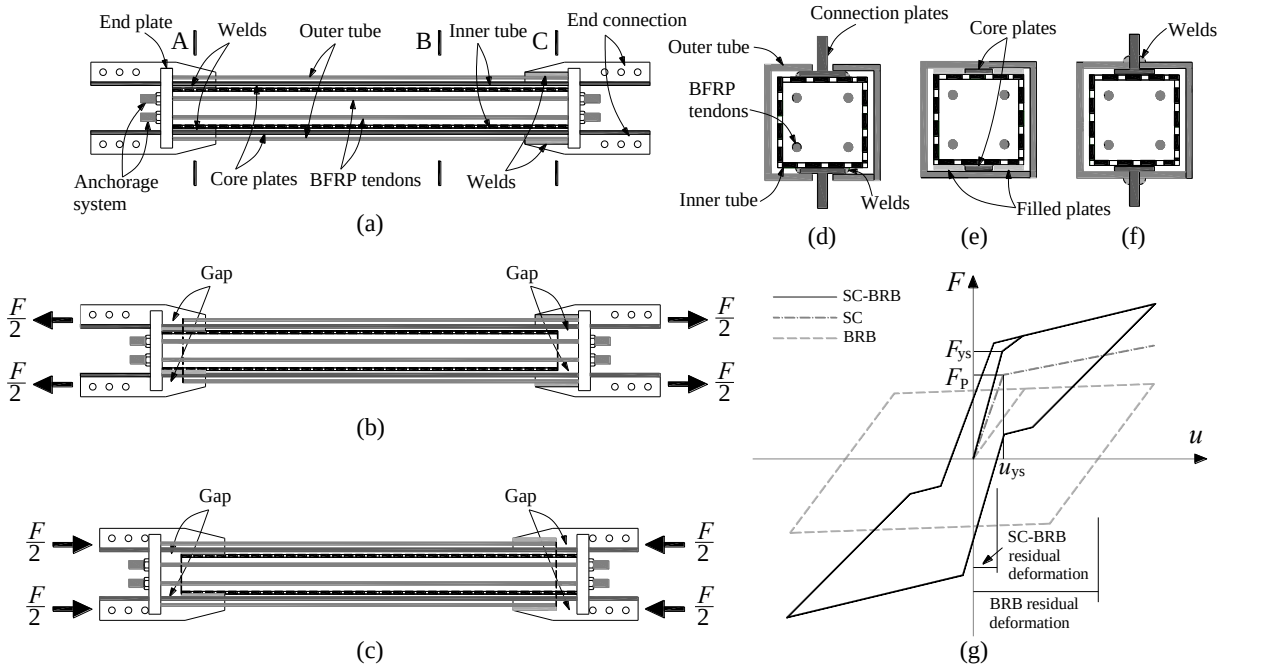

Fig. 1. – Concept diagrams of the dual-tube SC-BRB: (a) configuration; (b) in tension; (c) in compression; (d) section A; (e) section B; (f) section C; and (g) hysteresis curves

Fig. 1(g) shows the hysteresis curve of the dual-tube SC-BRB, which can be considered a superposition of the hysteresis curves of the BRB and the self-centering system. In the figure, u_{ys} is the activation displacement of the self-centering system and F_P is the pretension that is applied to the pretensioned tendons. Compared with the hysteresis curve of ordinary BRB, the hysteresis curve of the dual-tube SC-BRB exhibits a flag-shaped feature. When the applied pretension F_P is greater than the yield force of the core plates, the residual deformation of the brace will be less than u_{ys}, thereby realizing an ideal self-centering effect. The pretensioned tendon system is a key component for providing a restoring force to the self-centering structure. Therefore, to ensure the self-centering performance of the brace, it is necessary to systematically study the performance of the pretensioned tendon and its anchor.

3. Performance Test of the BFRP Tendon System

3.1 Specimen processing

Table 1 – Anchor types and sizes

Anchor type	Anchor length	Anchor inner diameter	Anchor outer diameter
Anchor A	350	20	32
Anchor B	350	18	32
Anchor C	380	18	32

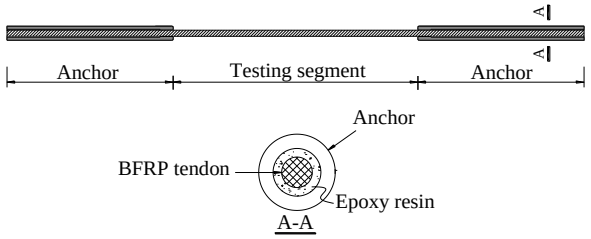

Fig. 2 – BFRP tendon specimen construction diagram

The nominal diameter of the BFRP tendon that is used in this test is ϕ14 mm (14-mm nominal diameter and a tendon area of 150.64 mm^2). Based on the previous research results[10], the basic

© The 17th World Conference on Earthquake Engineering

configuration of the anchor that is used in this experiment is illustrated in Fig.2 and three sets of anchors with various sizes are processed separately. The dimensions of the anchors are listed in Table 1.

Fig. 2 illustrates the construction of the BFRP tendon specimen. Based on the three sets of anchors in Table 1, a total of four batches of tests were conducted. The specimen numbers and related parameters of each batch are listed in Table 2. When anchoring the BFRP tendon, a colloid that is composed of an epoxy resin and a curing agent is used in the anchor.

3.2 Loading Protocol

The test uses a walter+bai hydraulic servo fatigue testing apparatus with a maximum load of 1000 kN and an actuator with a maximum load displacement of ±50 mm. When the specimen is installed, the upper and lower anchors of the specimen are clamped by hydraulic chucks. In the first and second batches of tests, to measure the deformation of the specimen testing segment, displacement gauges 1 and 2 were placed at the ends of the anchors near the specimen testing segment (Fig.3). The third batch of tests is a supplement to the second batch of tests and an extensometer was placed in the middle of the specimen testing segment to determine the change of the elastic modulus of the BFRP tendon during the test. In the fourth batch of tests, an extensometer was also set up and to obtain the relative displacement between the anchor and the tendon during the test, in addition to displacement gauges 1 and 2, displacement gauges 3 and 4 were added into the testing segment near the anchor (Fig. 3).

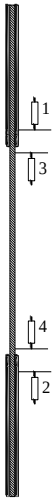

Fig. 3 – Displacement gauge arrangement

Table 2. Summary of basic information on the BFRP tendon specimens

Batch	Specimen number	BFRP diameter (mm)	Specimen length (mm)	Anchor type	Loading protocol
First batch	A-1	14	1260	Anchor A	Pro-2
	A-2	14	1260	Anchor A	Pro-2
Second batch	B-1	14	1260	Anchor B	Pro-2
	B-2	14	1260	Anchor B	Pro-2
Third batch	C-1	14	1260	Anchor B	Pro-2
	C-2	14	1260	Anchor B	Pro-2
	C-3	14	1260	Anchor B	Pro-3
Fourth batch	D-1	14	1320	Anchor C	Pro-1
	D-2	14	1320	Anchor C	Pro-2
	D-3	14	1320	Anchor C	Pro-3

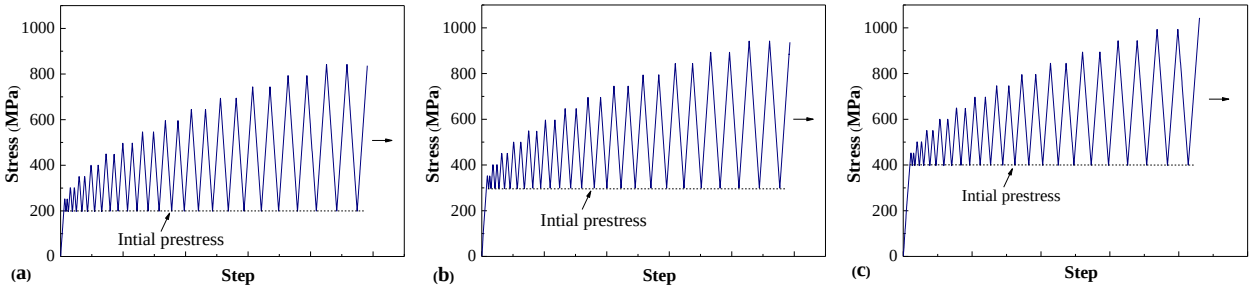

Fig. 4 – Testing protocols for the BFRP tendon specimens: (a) Pro-1; (b) Pro-2; and (c) Pro-3

The test uses a load-controlled loading method. To realize the stress state of the pretensioned tendons, the BFRP tendon specimen is pretensioned prior to cyclic loading. The test adopts three loading protocols (Fig.4): Pro-1, Pro-2 and Pro-3 apply initial prestresses of 200 MPa, 300 MPa and 400 MPa, respectively. Each loading protocol is incremented by 50 MPa amplitude, each amplitude is cycled twice, and the loading rate is 4 MPa/s. The loading protocol that is used for each specimen is listed in Table 2.

© The 17th World Conference on Earthquake Engineering

3.3 Test Results of the BFRP Tendon System

Table 3 summarizes the test results of the BFRP tendon specimen. The testing segment elongation is the difference between the testing segment length when the specimen was last unloaded to the initial prestress prior to the failure of the specimen and that at the start of the test. The ultimate elongation rate is the strain value of the BFRP tendon when the specimen is broken and is measured by an extensometer.

Table 3. Summary of the cyclic tensile test of the BFRP tendon specimen

Batch	Specimen number	Destructive form	Ultimate load (kN)	Testing segment elongation (mm)	Ultimate elongation rate (%)
First batch	A-1	Fracture	132	3.16	-
	A-2	Fracture	159	3.38	-
Second batch	B-1	Fracture	138	3.09	-
	B-2	Fracture	130	3.40	-
Third batch	C-1	Fracture	135	-	2.70
	C-2	Fracture	136	-	2.59
	C-3	Fracture	136	-	2.63
Fourth batch	D-1	Fracture	127	3.06	2.68
	D-2	Fracture	128	2.71	2.58
	D-3	Fracture	125	2.46	2.63

According to Table 3, the failure mode of all the specimens is the fracture of the BFRP tendon and no anchorage slippage occurs. Fig.5 and 6 show the load-strain curves of the BFRP tendon specimens in the third and fourth batches, respectively, of tests. $E_{p\text{-}in}$ is the elastic modulus of the BFRP tendon at the beginning of the test. The strains of the six specimens are linearly related to the applied load and the ultimate elongation rate (UER) exceeded 2.5% with little difference among specimens. The average value of $E_{p\text{-}in}$ of the third batch of specimens was 39.8 GPa and the average value of $E_{p\text{-}in}$ of the fourth batch of specimens was 37.2 GPa. Fig.5(d) and 6(d) show the changes in the elastic moduli of the third and fourth batches, respectively, at various test stages and E_p is the elastic modulus of the specimen at various test stages. The elastic modulus of each specimen changed very little throughout the test. The test results demonstrate that the material properties of BFRP tendons are highly stable during loading and are only slightly affected by the changes in the anchorage form and the loading protocol.

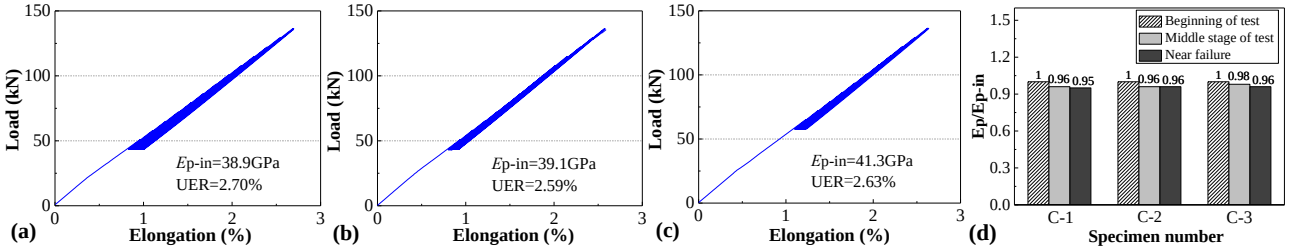

Fig. 5 – Load-strain curves of the third batch of specimens: (a) Specimen C-1; (b) Specimen C-2; (c) Specimen C-3; (d) Changes in the elastic modulus

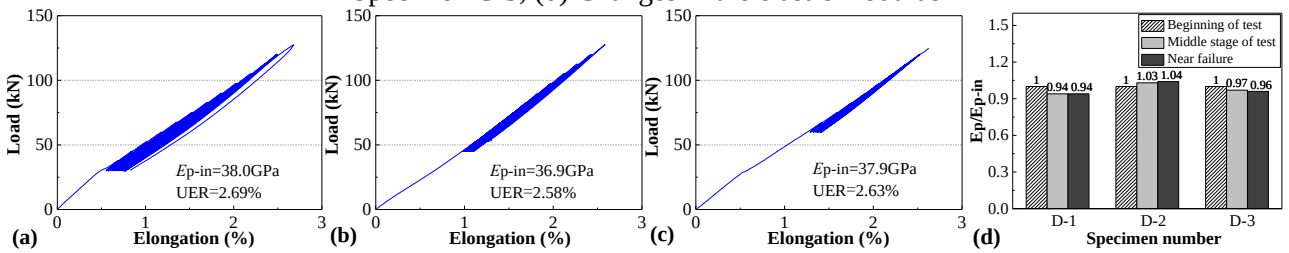

Fig. 6 – Load-strain curves of the fourth batch of specimens: (a) Specimen D-1 (b) Specimen D-2 (c) Specimen D-3 (d) Changes in the elastic modulus

© The 17th World Conference on Earthquake Engineering

Fig.7 shows the force-displacement curves of 7 BFRP tendon specimens in the first, second and fourth batches of tests. The displacement is measured by displacement gauges 1 and 2. The ultimate load of specimen A-2 is 159 kN, whereas the ultimate load of each remaining specimen is approximately 130 kN; hence, the ultimate load of the BFRP tendon has a dispersion. In the force-displacement curve, residual displacement occurs when the specimen is unloaded from the load amplitude to the initial prestress. Since the force-strain curve of the BFRP tendon corresponds to a linear elastic relationship, no substantial slippage damage between the tendon and the anchor is observed after the test. Therefore, we speculate that the residual displacement is caused by the relative displacement between the tendon and the anchor that is due to the colloidal deformation in the anchor when the specimen is stretched.

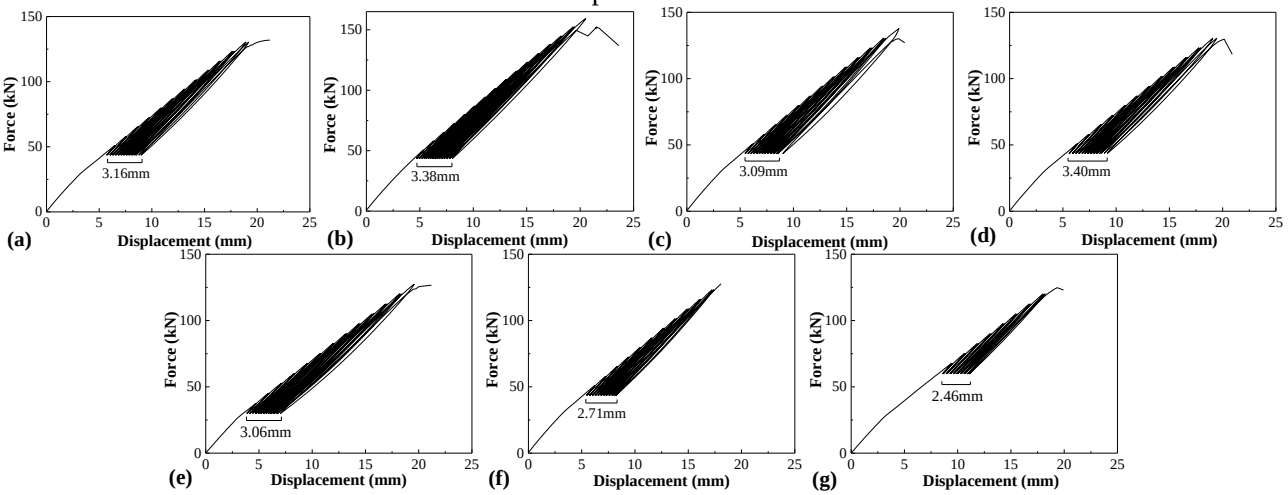

Fig. 7 – Force-displacement curves of the specimens: (a) Specimen A-1; (b) Specimen A-2; (c) Specimen B-1; (d) Specimen B-2; (e) Specimen D-1; (f) Specimen D-2; (g) Specimen D-3

According to Fig.3, the difference between the readings of displacement gauges 1 and 2 corresponds to the total residual deformation of the specimen (referred to as displacement gauge 1-2). The difference between the readings of displacement gauges 1 and 3 corresponds to the colloid deformation of the upper anchor (referred to as displacement gauge 1-3). The difference between the readings of displacement gauges 2 and 4 corresponds to the colloid deformation of the lower anchor (referred to as displacement gauge 2-4). The difference between the displacement gauge reading when the specimen is unloaded from a stress amplitude to the initial prestress and the corresponding reading at the beginning of the test is called the displacement difference. Fig.8(a), 8(b), and 8(c) present the stress amplitude-displacement difference curves of specimens D-1, D-2, and D-3, respectively. With the increase of the stress amplitude, the displacement differences of displacement gauges 1-2, 1-3 and 2-4 increase accordingly and the sum of the readings of displacement gauges 1-3 and 2-4 is close to that of displacement gauge 1-2; hence, the residual deformation of the specimen is caused by the colloid deformation in the upper and lower anchors.

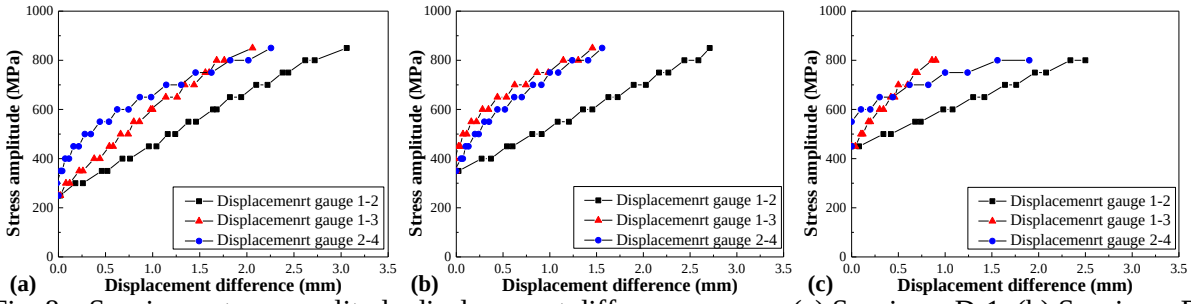

Fig. 8 – Specimen stress amplitude-displacement difference curves: (a) Specimen D-1; (b) Specimen D-2; (c) Specimen D-3

Due to the anchor colloidal deformation during the cyclic stretching of the BFRP tendon system, pretension loss is induced, which affects the self-centering performance of the SC-BRB. Therefore, further

© The 17th World Conference on Earthquake Engineering

study is needed to identify the key factors that affect the magnitude of the anchor colloidal deformation and to establish the corresponding regression formula to provide a basis for the design and performance evaluation of the brace.

3.4 Anchor Colloidal Deformation of the BFRP Tendon System Under Cyclic Loading

Define the anchor colloidal deformation ΔL_S as:

$$\Delta L_S = L_{S,\ \sigma i} - L_{S,\ \sigma 0} \tag{1}$$

where $L_{S,\ \sigma i}$ is the sum of the colloidal deformations of the anchors at both ends when the BFRP tendon specimens are unloaded from the stress amplitude to the initial prestress and $L_{S,\ \sigma 0}$ is the sum of the colloidal deformations of the anchors at both ends at the beginning of the test.

The stress difference is defined as the difference between the stress amplitude and the initial prestress during the test. The anchor colloidal deformation-stress difference curve of each specimen is plotted (Fig.9) and there is an strong linear relationship between the two parameters. Although the first and second batches of tests used the same loading protocol, the curves of the second batch of specimens, namely, B-1 and B-2, were consistent, while the curves of the first batch of specimens, namely, A-1 and A-2, differed. According to Table 3, the ultimate load of specimen A-2 is substantially higher than those of the other specimens and its performance is discrete. The three specimens of the fourth batch of tests were subjected to three loading protocols and the curves of specimens D-1, D-2 and D-3 in Fig.9(c) differed substantially. The curve slope of specimen D-1 was the smallest and the curve slope of specimen D-3 was the largest. According to the curves of the three specimens in the fourth batch of tests, with the increase of the initial prestress, the effect of the stress difference on the colloid deformation of the anchor increases gradually. Fig.9(d) compares the anchor colloidal deformation-stress difference curves of specimens A-1, B-2 and D-2. The loading protocols of the three specimens are the same; however, the sizes of anchors differ. The curves of the specimens in Fig.9(d) are approximately coincident; hence, the three anchor sizes that are considered in this paper yield the same control performance for the colloidal deformation of the anchors under the same loading protocol.

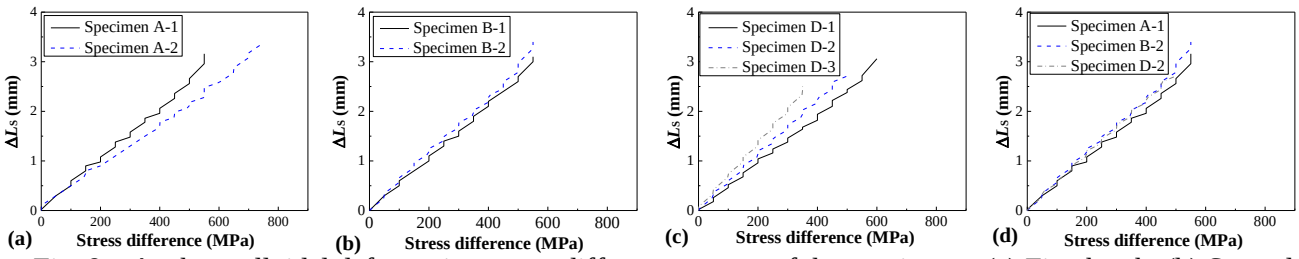

Fig. 9 – Anchor colloidal deformation-stress difference curves of the specimens: (a) First batch; (b) Second batch; (c) Fourth batch; (d) Specimens with various anchors under the same loading protocol

Under the same loading protocol, the anchor colloidal deformation-stress difference curves of specimens A-1, B-2 and D-2 are approximately coincident. In the fourth batch of specimens, the slope of the curve of specimen D-2 is between those of specimens D-1 and D-3. Therefore, this paper conducts linear regression based on the test curve of specimen D-2, determines the relationship between the anchor colloidal deformation ΔL_S and the stress difference $\Delta\sigma_a$, and obtains the regression formula.

$$\Delta L_S = 0.0055\Delta\sigma_a + 0.0353 \tag{2}$$

The units of ΔL_S and $\Delta\sigma_a$ are mm and MPa, respectively. Based on Eq. (2) and the properties of the BFRP tendon specimen, the pretension loss ΔF_P that is caused by the anchor colloidal deformation ΔL_S can be expressed as:

$$\Delta F_p = \frac{\Delta L_S}{L} E_{BFRP} A_{BFRP} \tag{3}$$

where L is the length of the testing segment of the BFRP tendon specimen and E_{BFRP} and A_{BFRP} are the elastic modulus and the sectional area, respectively, of the BFRP tendon. In this paper, only the performance testing of ϕ14 mm BFRP tendons and the adopted anchor is carried out. The same method can be used to test the BFRP tendons with various diameters.

© The 17th World Conference on Earthquake Engineering

4. Performance of the BFRP Tendon System in a Quasi-Static Test of SC-BRB

4.1 Specimen Design and Loading Protocol

The SC-BRB specimen is a 1/4-scale design of a single brace in a 12-story SC-BRB braced frame[17]. The total length of the specimen is 2500 mm. The self-centering system adopts four ϕ14 mm BFRP tendons and each pretensioned tendon applies a prestress of 45 kN. The core plate is composed of two Q235 steel plates (the yield strength is 249 MPa), each with a thickness of 8 mm and a width of 27 mm.

The SC-BRB specimen adopts the displacement control loading mode and the loading amplitudes are Δ_y, $2\Delta_y$, $3\Delta_y$, $4\Delta_y$, $5\Delta_y$, $6\Delta_y$, …; each amplitude is cycled twice and the loading rate is 0.1 mm/s. Δ_y=1.5 mm is the total bracing displacement at the yield of the core plates. The test is loaded until the specimen is broken. When the original structure has a story drift of 2%, the corresponding deformation requirement of the specimen after scaling is 18 mm.

4.2 Hysteretic Behavior of the SC-BRB Specimen

The test hysteresis curves of the SC-BRB specimen are plotted in Fig.10. In the initial stage of loading (Fig.10(a)), the hysteresis curve of SC-BRB has a substantial flag-shaped characteristic. When the displacement amplitude reaches 10.5 mm, the average value of the residual deformation (1.66 mm) is 15.8% of the displacement amplitude. As the displacement amplitude continues to increase, the residual deformation of the brace gradually increases due to the stress hardening of the core plate and the pretension loss. When the displacement amplitude reaches 18 mm (Fig.10(b)), the average value of the residual deformation (2.14 mm) is 11.9% of the displacement amplitude.

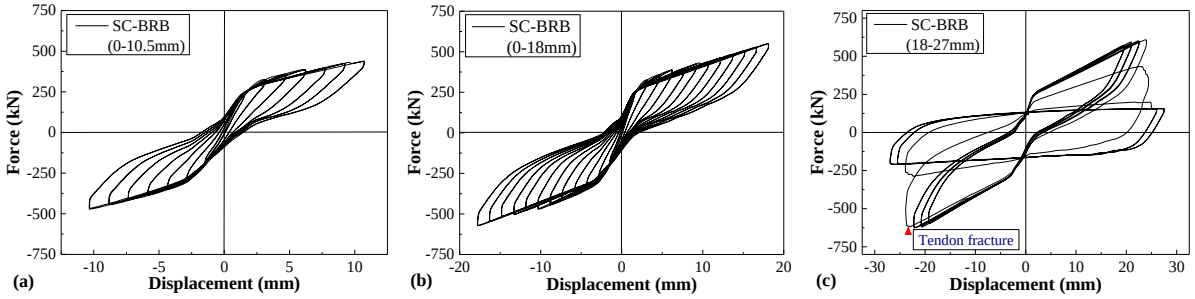

Fig. 10 – Test hysteresis curves of the SC-BRB specimen: (a) the initial-stage loading; (b) mid-stage loading; and (c) late-stage loading

Fig.10(c) shows the hysteresis curve of SC-BRB after the displacement amplitude exceeds 18 mm. In the process of increasing the displacement amplitude from 18 mm to 22.5 mm, the flag-shaped hysteresis performance of the brace remains relatively stable. When the displacement amplitude is 22.5 mm, the average residual deformation (3.55 mm) is 15.8% of the displacement amplitude and the brace bearing capacity doesn't decrease substantially. However, when the brace displacement is loaded to -23.64 mm, the brace axial force is rapidly reduced due to the fracture of part of the pretensioned tendons. When the displacement continues to load to 24.22 mm, the remaining pretensioned tendons also fracture. The specimens were subjected to two cycles of cyclic loading at the displacement amplitude of 25.5 mm and the brace was returned to the hysteretic characteristic of BRB.

4.3 Performance of the BFRP Tendon System

A prestress force of 45 kN was applied on each of the four BFRP tendons of the SC-BRB specimen. When the specimen was placed 5 days later for the test, the prestress forces were 42.2 kN, 39.4 kN, 40.1 kN and 40.8 kN, which correspond to losses of 6.2%, 12.4%, 10.9% and 9.3%, respectively.

Fig.11 presents the hysteresis curves of four BFRP tendons. During the deformation of the brace, the tendons are always stretched long and the bearing capacity does not decrease substantially prior to the fracture of the tendons. The hysteretic curves of the four BFRP tendons gradually shifted downward during the test, which corresponds to pretension being lost. The performance tests of the BFRP tendon systems

© The 17th World Conference on Earthquake Engineering

demonstrate that the pretension loss is caused by the anchor colloidal deformation. During the test of SC-BRB, the maximum internal forces of the four tendons were 124.3 kN, 108.4 kN, 112 kN and 116.3 kN. The pretension losses of the four tendons after unloading from the maximum internal force were 16.8 kN, 14.2 kN, 14.8 kN and 15.5 kN compared with the beginning of the test. The pretension losses of BFRP-1, BFRP-2, BFRP-3 and BFRP-4 can be estimated via Eq. (3) as 16.8 kN, 14.2 kN, 14.8 kN and 15.5 kN, respectively, and the ratios to the actual loss are 150%, 106%, 102% and 100%, respectively. In addition to BRFP-1, the pretension loss evaluation values of the other three tendons accord with the actual values.

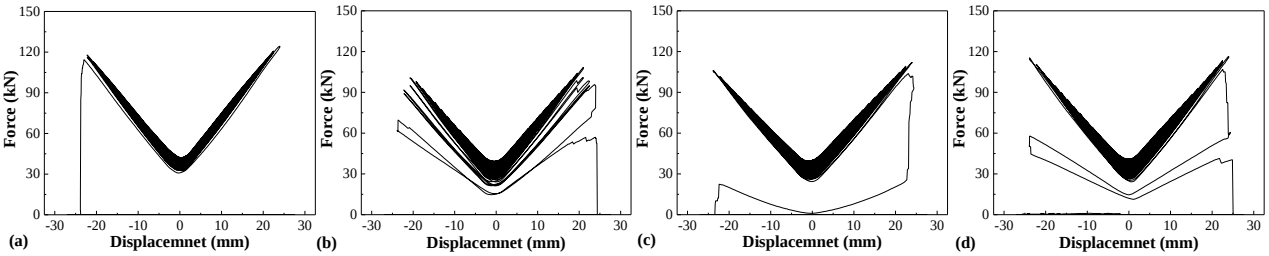

Fig. 11 – Hysteresis curves of four BFRP tendon systems in the SC-BRB specimen: (a) BFRP-1; (b) BFRP-2; (c) BFRP-3; and (d) BFRP-4

5. SC-BRB Rheological Model that Considers the Anchor Colloidal Deformation

To simplify the analysis of the structural hysteresis performance and the structural seismic performance, based on rheological analysis theory, Zhou et. al.[18] established a rheological model that can describe the hysteretic behavior of SC-BRB. Since the anchor colloidal deformation is not considered when the rheological model is established, which will affect the analysis accuracy, the regression formula of the anchor colloidal deformation is introduced into the SC-BRB rheological model equation.

5.1 Establishing an SC-BRB Rheological Model that Considers the Anchor Colloidal Deformation

When establishing the SC-BRB rheological model (Fig.12), the governing equations should be determined separately for the BRB part and the self-centering (SC) part. The SC part is simulated by connecting spring SC1 in series with the friction element and in parallel with spring SC2. The activation force F_t of the friction element is used to represent the applied initial prestress force F_P. When the brace displacement u exceeds the activation displacement u_{ys}, spring SC1 stops deforming and the displacement is provided by the friction element. In addition, the connecting ends of the brace are simulated by spring 2, which is connected with the main structure of the brace in series. To consider the effect of the anchor colloidal deformation, this paper introduces Eq. (2) when establishing the governing equation of the SC part.

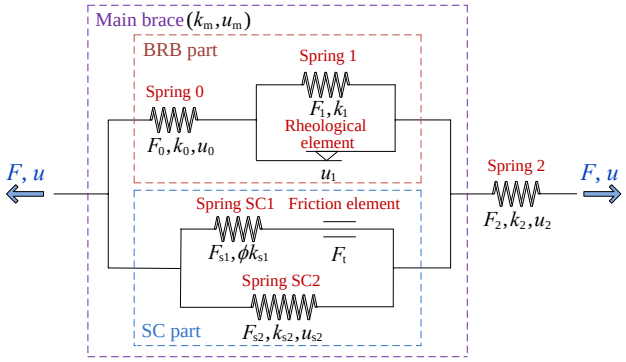

Fig. 12 – Rheological model of SC-BRB

In Fig.12, u_{s2} represents the deformation of the SC system and u_2 represents the displacement of the connecting ends. F_{s2} and F_2 are the forces that are caused by the corresponding displacement, F_{s1} is the bracing load on the inner and outer tubes, and F_t represents the pretension on the inner and outer tubes. k_{s1} is the stiffness of the inner and outer tubes, k_{s2} is the stiffness of the pretensioned tendons, and k_2 is the stiffness of the connecting ends. Research[19] shows that due to the tube length tolerances, the test value of the initial

© The 17th World Conference on Earthquake Engineering

stiffness of the SC-BRB specimen is smaller than the theoretical value; hence, the tube stiffness modification coefficient ϕ is introduced into the model.

According to Fig.12, the SC part force F_s is the sum of the inner and outer tube force F_{s1} and the force of the pretensioned tendons F_{s2}:

$$F_s = F_{s1} + F_{s2} \tag{4}$$

The calculation can be divided into two stages:

In the first stage, the brace displacement is less than u_{ys}, which is composed of the activation displacement of the main brace u_{mys} and the displacement of the connecting ends under F_P:

$$u_{ys} = u_{mys} + u_{2ys} = \frac{F_P}{\phi k_{s1} + k_{s2}} + \frac{F_P}{k_2} + \frac{F_P k_{BRB}(t)}{k_2\left(\phi k_{s1} + k_{s2}\right)} \tag{5}$$

The restoring force of the SC part can be calculated via the following formula:

$$F_s = (\phi k_{s1} + k_{s2}) u_{s2}(t) \tag{6}$$

In the second stage, the brace displacement exceeds u_{ys}. The inner and outer tubes begin to slide relatively and the stiffness of the SC part is only the stiffness of the pretensioned tendons:

$$k_s = k_{s2} \tag{7}$$

According to the two cases of the brace in tension and compression, F_s can be calculated as follows:

$$\begin{aligned} &\text{If } u(t) > u_{ys}, \quad F_s = k_{s2}\left(u_{s2}(t) - \frac{F_P}{\phi k_{s1} + k_{s2}}\right) + F_P \\ &\text{If } u(t) < -u_{ys}, \quad F_s = k_{s2}\left(u_{s2}(t) + \frac{F_P}{\phi k_{s1} + k_{s2}}\right) - F_P \end{aligned} \tag{8}$$

Based on Eq. (2) and considering the influence of the anchor colloidal deformation, the prestress force F_P of the SC part can be calculated as:

$$F_P = F_{P0} - \left[0.0055\left(F_{s,\max} - F_{P0}\right)/A_p + 0.0353\right]F_{s2} \tag{9}$$

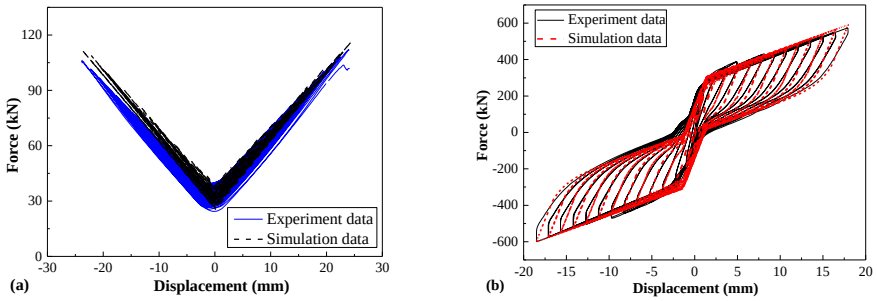

Fig. 13 – Comparison between test results and simulation results that are based on the rheological model: (a) The force-displacement curve of BFRP-3 and (b) the hysteresis curve of SC-BRB

The rheological model that considers the anchor colloidal deformation was used to simulate the SC-BRB specimen. Fig.13(a) compares the force-displacement curves of BFRP-3. The simulated curve not only matches the test curve but also effectively reflects the pretension loss. In Fig.13(b), the rheological model that considers the anchor colloidal deformation can accurately simulate the hysteretic performance of SC-BRB with the BFRP tendon system.

5.2 Influence of the Anchor Colloidal Deformation on the SC-BRB Hysteretic Performance

The rheological models of the SC-BRB specimen without (Model A) and with (Model B) consideration of the anchor colloidal deformation were established. Fig.14(a) compares the brace hysteresis curve for displacement amplitudes of less than or equal to 24 mm. The stiffnesses of the two groups of curves are approximately the same at each stage. However, due to the pretension loss that is caused by the anchor colloidal deformation, the bearing capacity of Model B is smaller than that of Model A, while the residual deformation is larger and the difference increases with the increase of displacement amplitude.

© The 17th World Conference on Earthquake Engineering

Fig.14(b) compares the hysteresis curves of the self-centering system. The anchor colloidal deformation doesn't affect the stiffness of the self-centering system; however, it will reduce the activation force and the activation displacement and lead to the reduction of the bearing capacity of the self-centering system after activation. When the displacement amplitude reaches 24 mm, the maximum bearing capacity of the self-centering system of Model B decreases by 48 kN compared with that of Model A. The SC-BRB hysteresis curve with a displacement amplitude of 24 mm is extracted (Fig.14(c)) and the maximum bearing capacity of Model B is reduced by 48 kN compared with Model A, which is consistent with the difference of the self-centering system. In addition, when the load is unloaded to 0, the mean residual deformation of Model B is increased by 90% compared to Model A.

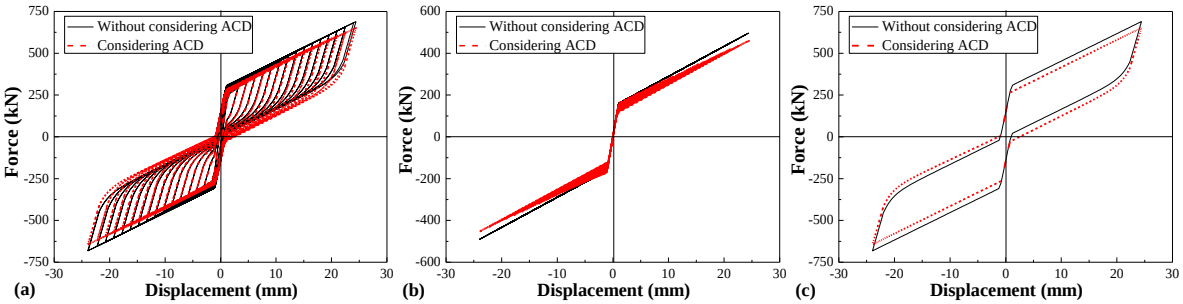

Fig. 14 – Comparison of the rheological model simulation results without and with consideration of the anchor colloidal deformation (ACD): (a) The hysteresis curve of SC-BRB; (b) the hysteresis curve of the self-centering system; and (c) the SC-BRB hysteresis curve of 24 mm displacement amplitude

6. Conclusions

(1) The ultimate elongation rate of BFRP tendons that was measured via the cyclic tensile test exceeds 2.5%. In addition, the elastic modulus of each BFRP tendon specimen changes very little throughout the test and is highly stable.

(2) The anchors that are used in this paper can effectively anchor the BFRP tendons. However, the tests have demonstrated that the colloid in the anchor will deform under the action of a cyclic tensile load. The experimental analysis demonstrates that there is a clear linear relationship between the anchor colloidal deformation and the stress difference (the difference between the stress amplitude and the initial prestress) and the regression formula of the anchor colloidal deformation is established based on the test results.

(3) The BFRP tendon system can provide a reliable self-centering restoring force for the SC-BRB. However, during the quasi-static test of SC-BRB, the BFRP tendon system has a pretension loss that is due to the anchor colloidal deformation and the regression formula of the anchor colloidal deformation can be used to accurately evaluate the pretension loss.

(4) An SC-BRB rheological model that considers the anchor colloidal deformation is established, and the model can accurately simulate the hysteretic performance of the brace. The hysteretic behavior analysis of SC-BRB that is based on rheological model demonstrates that the anchor colloidal deformation will lead to a decrease in the brace bearing capacity and an increase in the residual deformation and that the effect will strengthen with the increase in the displacement amplitude.

7. Acknowledgements

The research described in this paper was sponsored by "High-level Talent Research Funding Project of Guizhou Institute of Technology" (XJGC20190907). The supports are gratefully acknowledged.

8. References

[1] Dyke, SJ (2010): 2020 vision for earthquake engineering research: Report on an openspace technology workshop on the future of earthquake engineering. ⟨http://nees.org/resources/1636⟩ (Nov. 3, 2010).

© The 17th World Conference on Earthquake Engineering

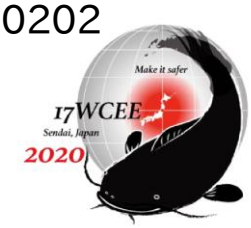

[2] NIED and NEES Consortium. (2010). Report of the Seventh Joint Planning Meeting of NEES/E: Defense Collaborative Research on Earthquake Engineering. PEER 2010/109. Berkeley, CA: University of California at Berkeley.

[3] McCormick J, Aburano H, Ikenaga M, Nakashima M (2008): Permissible residual deformation levels for building structures considering both safety and human elements. *Proc., 14th World Conf. on Earthquake Engineering*, Beijing.

[4] Yang CSW, DesRoches R, Leon RT (2010): Design and analysis of braced frames with shape memory alloy and energy-absorbing hybrid devices. *Eng. Struct*., 32(2), 498-507.

[5] Xu LH, Fan XW, Li ZX (2016): Development and experimental verification of a pre-pressed spring self-centering energy dissipation brace. *Eng. Struct*., 127, 49-61.

[6] Christopoulos C, Tremblay R, Kim HJ, Lacerte M (2008): Self-centering energy dissipative bracing system for the seismic resistance of structures: Development and validation. *J. Struct Eng.*, 10.1061/ (ASCE)0733-9445(2008)134:1(96), 96–107.

[7] Miller DJ, Fahnestock LA, Eatherton MR (2012): Development and experimental validation of a nickel–titanium shape memory alloy self-centering buckling-restrained brace. *Eng. Struct*., 40, 288-298.

[8] Wu G, Dong ZQ, Wang X, Zhu Y, Wu ZS (2014): Prediction of long-term performance and durability of BFRP bars under the combined effect of sustained load and corrosive solutions. *J. Compos. Constr.*, 19(3), 04014058.

[9] Zhou Z, He XT, Wu J, Wang CL, Meng SP (2014): Development of a novel self-centering buckling-restrained braces with BFRP composite tendons. *Steel Compos. Struct*., 16(5), 491–506.

[10] Zhou Z, Xie Q, Lei XC, He XT, Meng SP (2015): Experimental investigation of the hysteretic performance of dual-tube self-centering buckling-restrained braces with composite tendons. *J. Compos. Constr.*, 10.1061/(ASCE)CC.1943-5614.0000565, 04015011.

[11] Chou CC, Chung PT (2014): Development of cross-anchored dual-core self-centering braces for seismic resistance. *Journal of Constructional Steel Research*, 101, 19-32.

[12] Bruce TL, Eatherton MR (2016): Behavior of post-tensioning strand systems subjected to inelastic cyclic loading. *J. Struct Eng*., 142(10), 04016067.

[13] El RA (2013): Durability and fatigue of basalt fiber-reinforced polymer bars gripped with steel wedge anchors. *J. Compos. Constr.*, 10.1061/(ASCE)CC.1943-5614.0000417, 04013006.

[14] Wang X, Shi J, Wu Z, Zhu Z (2015): Fatigue behavior of basalt fiber-reinforced polymer tendons for prestressing applications. *J. Compos. Constr*., 20(3), 04015079.

[15] Wang X, Xu P, Wu Z, Shi J (2015): A novel anchor method for multitendon FRP cable: Manufacturing and experimental study. *J. Compos. Constr*., 19(6), 04015010.

[16] Shi J, Wang X, Wu Z, Zhu Z (2015): Effects of radial stress at anchor zone on tensile properties of basalt fiber-reinforced polymer tendons. *Journal of Reinforced Plastics and Composites*, 34(23), 1937-1949.

[17] Xie Q, Zhou Z, Huang JH, Meng SP (2016): Influence of tube length tolerance on seismic responses of multi-storey buildings with dual-tube self-centering buckling-restrained braces. *Eng. Struct.,* 116, 26-39.

[18] Zhou Z, Xie Q, Meng SP, Wang WY, He XT (2016): Hysteretic performance analysis of self-centering buckling restrained braces using a rheological model. *J. Eng. Mech.*, 10.1061/(ASCE)EM.1943-7889.0001080, 04016032.

[19] Erochko J, Christopoulos C, Tremblay R (2014): Design, testing, and detailed component modeling of a high-capacity self-centering energy-dissipative brace. *J. Struct Eng*., 141(8), 04014193.

© The 17th World Conference on Earthquake Engineering